



Cite this: *Nanoscale*, 2016, **8**, 17881

Hydro-actuation of hybrid carbon nanotube yarn muscles†

Xiaogang Gu,^{a,b,c} Qingxia Fan,^{a,b,c} Feng Yang,^{a,b,c} Le Cai,^{a,b} Nan Zhang,^{a,b,c} Wenbin Zhou,^{a,b} Weiya Zhou^{*a,b,c} and Sishen Xie^{*a,b,c}

Hybrid hydro-responsive actuators are developed by infiltrating carbon nanotube yarns using poly(3,4-ethylenedioxythiophene):poly(styrenesulfonate). These actuators demonstrate impressive rotation and contraction in response to water due to volumetric expansion of the helical arrangement of carbon nanotubes. The total torsional stroke is 3720 revolutions per m and the simultaneously generated contractive strain reaches 24% at a paddle-to-yarn mass ratio of 350. The contraction output can furthermore be significantly enhanced by constraining the rotational motion and it reaches 68% with an applied stress of 1 MPa. Additionally, hybrid yarns exhibit an approximately linear response to humidity changes and show extra capability of electrical actuation, which, combined with the excellent hydro-actuation performance, endow them with great potential for a variety of applications including artificial muscles, hydro-driven generators, moisture switches and microfluidic mixers.

Received 4th August 2016,
Accepted 9th September 2016

DOI: 10.1039/c6nr06185k

www.rsc.org/nanoscale

Introduction

Carbon nanotube (CNT) yarn-based actuators have attracted considerable interest because of their potential applications as artificial muscles or microelectromechanical devices.^{1–14} The helical-structured yarns can reversibly generate rotation and contraction due to dimensional changes caused by various external stimuli (ions, current, light, solvents, vapours, *etc.*). Several elegant designs^{1,2,6} have been reported over the past few years, but they still suffer from relatively low torsional stroke, poor specific work capacity or marginal stability in air. Recently, a new type of hierarchically organized multi-ply CNT yarn actuator driven by adsorption of ethanol or its vapours

has been created and it exhibited excellent performance.¹⁰ Nevertheless, resulting from the hydrophobic characteristic of pristine CNTs, little actuation will be obtained if the trigger is changed to water or environmental humidity, which though is more widely accessible. To address this issue and realize moisture-responsive CNT yarns, surface modification by oxygen plasma¹¹ has been carried out. However, this technique tends to cause severe damage to CNTs on more intense treatment and consequently decreases their mechanical strength. The hydrophobicity inside the primary yarns, furthermore, can hardly be influenced to participate in actuation. Besides this effort, poly(diallyldimethylammonium) chloride (PDDA) has also been adopted to build humidity-driven CNT yarn actuators,¹² but the highly-soluble PDDA can dissolve if the yarn muscles are immersed into liquid water for possible situations in the future application, which will result in their degradation, because the interaction between pure PDDA and non-oxidized CNTs is very weak.¹⁵ In this work, we construct hybrid muscles by infiltrating the CNT yarns with the hygroscopic and more stable poly(3,4-ethylenedioxythiophene):poly(styrenesulfonate) (PEDOT:PSS). The moisture-sensitive guest materials are uniformly embedded in the twist-spun yarns with high specific strength, and their hybrids provide large-stroke and reversible actuation once they come into contact with water.

Results and discussion

The hybrid yarns were assembled from freestanding single-walled carbon nanotube (SWCNT) films, which were fabricated

^aBeijing National Laboratory for Condensed Matter Physics, Institute of Physics, Chinese Academy of Sciences, Beijing 100190, China. E-mail: wyzhou@iphy.ac.cn, sxxie@iphy.ac.cn

^bBeijing Key Laboratory for Advanced Functional Materials and Structure Research, Beijing 100190, China

^cUniversity of Chinese Academy of Sciences, Beijing 100049, China

†Electronic supplementary information (ESI) available: Calculation details, optical photograph and SEM image of the pristine SWCNT film, Raman spectra of the pristine SWCNT film, SEM images of the pure yarn and the hybrid yarn with a core-shell structure, optical photograph for contraction with different applied stresses, feedback by the laser displacement sensor of the whole rotating process, typical stress-strain curves of pristine and hybrid yarns, photograph of a homemade humidity control system and relative humidity/temperature variation in the humidity chamber, torsional stroke of CNT/PEDOT:PSS and CNT/PDDA hybrid yarns before and after being soaked in water for 24 hours, comparison between the as-prepared hybrid CNT/PEDOT:PSS yarn actuator and the previously reported CNT yarn-based actuators, and demo videos of the actuators. See DOI: 10.1039/c6nr06185k

through the floating catalyst chemical vapour deposition (FCCVD) method.¹⁶ The film, composed of entangled strongly-bonded SWCNT bundles, features a hierarchical reticulate architecture (Fig. S1†) with ultrathin thickness (~ 200 nm), large area (dozens to hundreds of square centimetres), and high mechanical strength (360 MPa) and electrical conductivity (~ 2000 S cm^{-1}).¹⁶ Our previous work shows that this kind of directly grown SWCNT films are excellent material platforms for a wide range of functional devices, including super-fast ionic actuators,¹⁷ high-performance electrochemical capacitors^{18–20} as well as super-stretchable elastic conductors²¹ and strain sensors.²²

Briefly, in the process of constructing the hybrid yarns, a narrow rectangular ribbon (3–5 mm in width) cut from the SWCNT film was firstly put into and blended with the commercially available PEDOT:PSS aqueous solution and then drawn out (Fig. 1a, left). Subsequently, the infiltrated ribbon was transformed into a yarn (typically, 25–50 μm in diameter, 8000–10 000 turns per m in twist density) by controlled motor-twisting (Fig. 1a, right and Video S1†). In order to obtain a helical yarn which is crucial to torsional and contractive actuation, it is indispensable to do the twisting before it dries. Once the degree of twisting exceeds a critical value (~ 8000 turns per m in our case), the formation of a spring-like coiled structure is initiated (Fig. 1b, middle); continued spinning makes the coils more densely packed (Fig. 1b, right) and the yarn length shorter. Moreover,

the porous feature at the surface and inside of the as-prepared hybrid yarns (Fig. 1c), which is supposed to not only enable rapid actuation but also permit fast recovery, serves as another prerequisite of vital importance for the desired performance. It is noteworthy that infiltration before twist-insertion is essential to create the surface pores. In contrast, a core-shell structure would otherwise be formed, in which a dense PEDOT:PSS layer wraps up the CNT yarn and thus unfavourably restrains its actuation (Fig. S3 and Video S2†).

A paddle was attached to the free end of the yarn for convenient observation and measurement. The hybrid yarns exhibit remarkable torsional stroke and contractive strain triggered by water (see Video S3†). For a coiled yarn that was 25 mm in length, 85 μg in weight and 9736 turns per m in twist density, rotation and contraction (Fig. 2a and S4†) occurred simultaneously, when a water droplet moved up and down along the yarn's lengthwise direction until it was water saturated. The total torsional stroke was 93 revolutions (3720 revolutions per m, $1339^\circ \text{mm}^{-1}$), corresponding to 38% of the complete inserted twist, even though the paddle was 350 times as heavy as the yarn. Meanwhile, the generated contractive strain (defined as the percentage of contraction to initial yarn length) reached 24%. In spite of the paddle with a much higher moment of inertia ($I = 4.9 \times 10^{-10}$ kg m^2), the rotation of our hybrid yarn is so outstanding that it is nearly twice the value of the ethanol-actuated hierarchically arranged helical

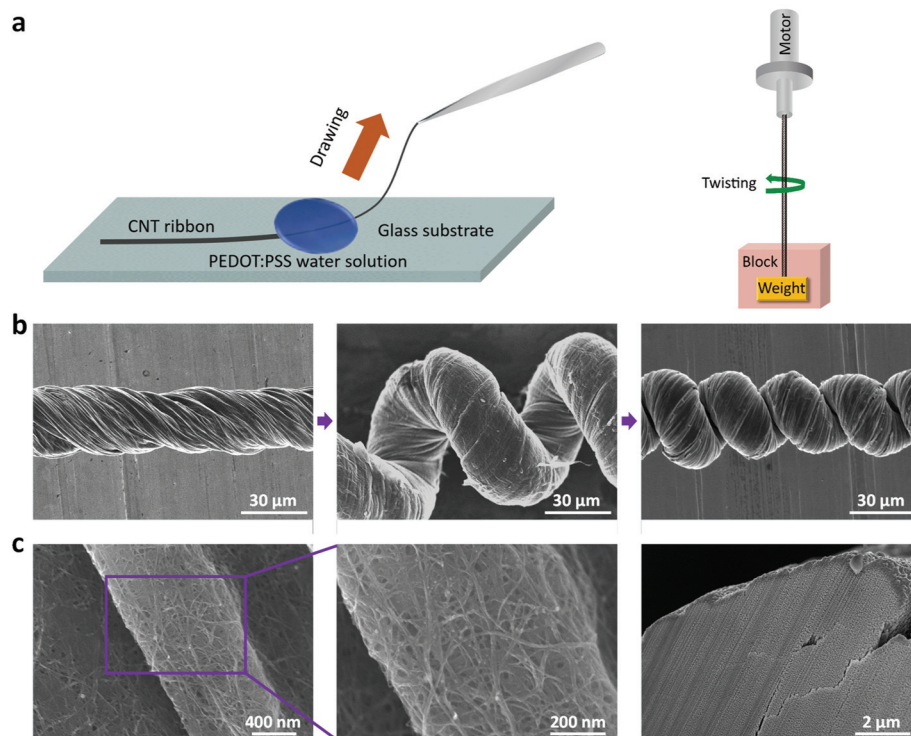


Fig. 1 (a) Schematic illustration of hybridization and twist-insertion process. The CNT ribbon is drawn out from a drop of PEDOT:PSS aqueous solution (left) and motor-twisted after infiltration (right). A block is utilized to keep the weight from rotating. (b) The evolution of yarn coiling feature with increasing twist density. The hybrid yarn transforms from non-coiled (left) to loosely coiled (middle) and then to compactly coiled (right) with continuous twisting. The twist density was calculated based on the original length of the hybrid yarn. (c) SEM images of the surface (left and middle) and cross-section (right) of the hybrid yarn.

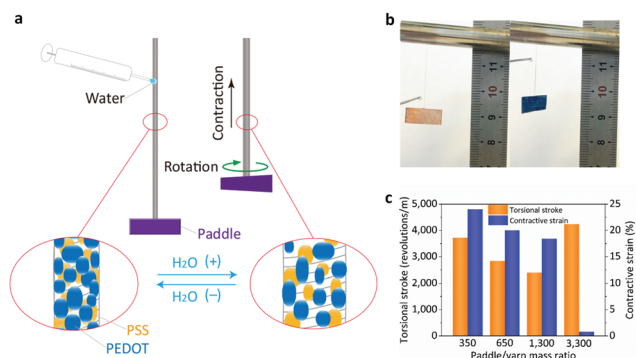


Fig. 2 (a) Actuation mechanism of the hybrid yarns. Rotation and contraction are produced due to water adsorption of PEDOT:PSS that induces swelling and untwisting of the helical yarns. (b) Paddle's position before (left) and after (right) actuation. The paddle-to-yarn mass ratio is 650. The contractive strain is ~20%. (c) Paddle mass dependence of total torsional stroke and contractive strain. The hybrid yarn for (b) and (c) is 25 mm in length, 85 μg in weight and 9736 turns per m in twist density.

fibre (HHF, 2050 revolutions per m, $I = 2 \times 10^{-10} \text{ kg m}^2$),¹⁰ 5 times more than the liquid-phased, electrochemically-actuated yarn ($250^\circ \text{ mm}^{-1}$, $I = 2 \times 10^{-10} \text{ kg m}^2$),¹ and 3–5 orders of magnitude higher than the results obtained for torsional actuators based on shape-memory alloys ($0.15^\circ \text{ mm}^{-1}$),²³ piezoelectric ceramics ($0.008^\circ \text{ mm}^{-1}$)²⁴ and conducting polymers ($0.01^\circ \text{ mm}^{-1}$).²⁵ Furthermore, the contraction (20%, the paddle-to-yarn mass ratio was 650) is twice the value reported for the HHF (10%, the paddle-to-yarn mass ratio was 570).¹⁰ As indicated in Fig. 2b, the yarn untwists and contracts less with increase in the mass of the paddle. However, when the paddle ($I = 4.6 \times 10^{-9} \text{ kg m}^2$) was 3300 times the mass of the yarn, even though the contractive strain was only 0.8%, the total torsional stroke rose to 106 revolutions, which is probably because the paddle was so heavy that contraction had been greatly limited and substantial work had been carried out for its rotation. This phenomenon in turn also inspired us to amplify the contraction output by constraining the rotation, which is investigated in the following experiment.

Previous studies have demonstrated that the coiled structure like that in our hybrid yarns is helpful to significantly enhance the contractive strain.^{2,6,8,10} Apart from this, to fully realize the potential of lengthwise contraction, herein, a piece of glass slide was utilized to prevent the paddle from rotating successively (Fig. 3a). By this configuration, the yarn rotated the paddle slightly and lifted it upward once it came into contact with a water droplet (Fig. 3b and Video S4†). Besides the twist density, the contractive strain and the work capacity are both stress-dependent (Fig. 3c). For a coiled yarn that was 29 mm in length and 9972 turns per m in twist density, the paddle corresponding to the minimum applied stress of about 1 MPa (paddle-to-yarn mass ratio was 506) had the maximum contraction of 68% (Fig. S5†). The specific work capacity was calculated to be 96.9 J kg^{-1} , omitting some negligible energy consumption from friction and rotation, which is still 3 times more than the result of the ethanol-actuated HHF

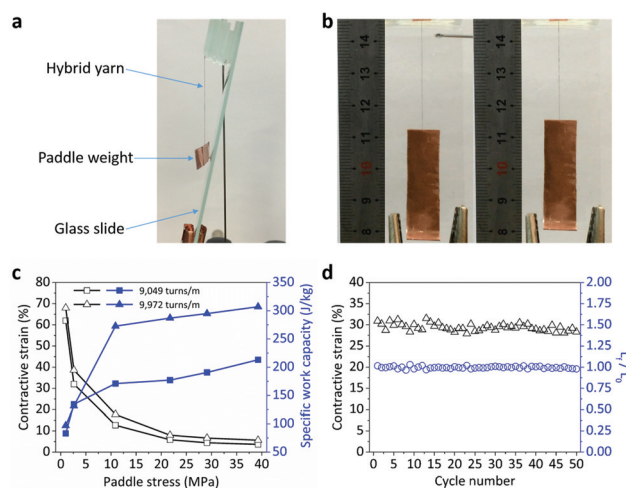


Fig. 3 (a) Side-view of the experimental setup for enhancing the contraction output. The successive rotation of the paddle is impeded by a piece of an inclined glass slide. (b) Paddle's position before (left) and after (right) actuation. The paddle-to-yarn (9972 turns per m) mass ratio is 11 039. The contractive strain is ~9.4%. (c) Stress dependence of the contractive strain and specific work capacity. The mass of the two yarns under ambient conditions is 141 μg (9972 turns per m) and 124 μg (9049 turns per m), respectively. (d) Cycling test of the contractive performance. The yarn (9049 turns per m) is repeatedly actuated to the maximum contraction. The paddle-to-yarn mass ratio is 1524. L_0 and L_t denote the yarn length before and after each actuation, respectively.

(26.7 J kg^{-1})¹⁰ and 12 times that of typical mammalian skeletal muscles (7.7 J kg^{-1}).²⁶ Moreover, the contractive stress generated by the hybrid yarn reached more than 39 MPa, which is nearly twice as powerful as the moisture-actuated plasma-treated yarn (22.4 MPa at an oxygen content of 17.5%),¹¹ 35 times the stress reported for the HHF ($\sim 1.1 \text{ MPa}$, measured by clamping the two ends)¹⁰ and 110 times more than the maximum stress generated by skeletal muscles (0.35 MPa).²⁶ In addition, the contractive performance is proved to be robust and reproducible from the fatigue test, where the hybrid yarn (9049 turns per m) was repeatedly actuated to the maximum strain with an applied stress of $\sim 2.6 \text{ MPa}$ (see Video S5†). As displayed in Fig. 3d, during 50 cycles of actuation, the contractive strain remains constant around 30% with the variation range less than 2%, and the initial length is close to be completely restored after removing the water droplet.

Although a large twist density means powerful untwisting capacity, coiling is not necessary for a fast and large rotation. In fact, regarding our hybrid CNT yarns, the closely-packed coils would impede rotation if the paddle is too light to separate them apart (Fig. 4c). For a non-coiled yarn that was 45 mm in length and 8032 turns per m in twist density, the paddle ($I = 1.8 \times 10^{-10} \text{ kg m}^2$) rotated vigorously once the yarn was brought into contact with a water droplet. Creatively, a laser displacement sensor was employed to track and record the paddle's rotation (Fig. 4a, S6a† and Video S6†), given that the position of the laser spot would change periodically with the rotation of the targeted paddle. The forward and reverse rotation could also be readily distinguished from the wave

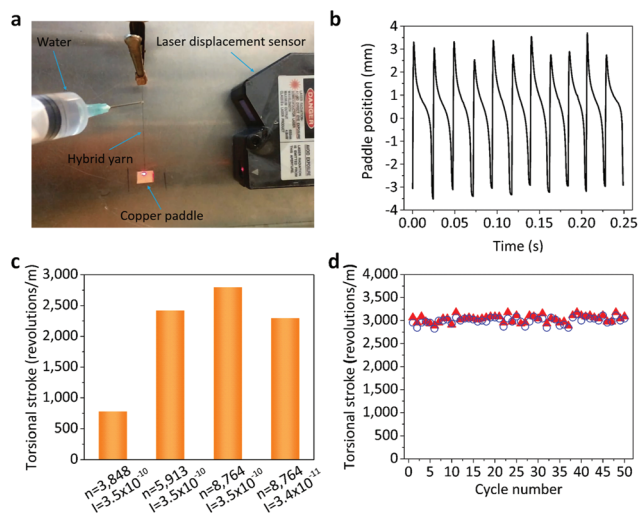


Fig. 4 (a) Experimental set-up for rotation recording. The paddle is placed in the effective detection range of the laser displacement sensor. The position changes of the laser spot on the targeted paddle accurately reflect its periodical rotation. (b) Wave pattern of the rotating paddle when approaching the maximum rotation velocity. The adjacent peaks or valleys correspond to the rotation of a half-cycle. (c) Torsional stroke versus n and I . n and I denote the twist density of the yarn and paddle's moment of inertia with the units, turns per m and kg m^2 , respectively. (d) Cycling test of the torsional performance. The yarn is repeatedly stimulated to the maximum rotation. Solid red triangles and hollow blue circles are for the forward and reverse rotation, respectively.

pattern (Fig. S6b and c†). This approach is more efficient and accurate than the conventionally used videoframe-based method. Derived from the minimum rotation period of 43 ms (Fig. 4b), the peak rotation velocity reached 1395 rpm (31 000 rpm per meter), which is nearly 5 times the value reported for the HHF (6361 rpm per meter)¹⁰ and 3 times more than that of the liquid-phased, electrochemically-actuated yarn muscle (9833 rpm per meter),¹ based on a similar moment of inertia ($\sim 2 \times 10^{-10} \text{ kg m}^2$). The initially released specific torque was estimated to be 0.52 N m kg^{-1} , which is about 6 times the result of the graphene fibre motor ($0.082 \text{ N m kg}^{-1}$)²⁷ and comparable to that of the HHF (0.63 N m kg^{-1})¹⁰ or the hydrophilic secondary fibre (0.4 N m kg^{-1}).¹¹ To evaluate the durability and reversibility of the torsional performance, we repeatedly actuated the yarn to the maximum rotation of 50 cycles, where the total torsional stroke was maintained around 135 revolutions (3000 revolutions per m) without any significant degradation of both forward and reverse rotations (Fig. 4d).

The moisture-excited rotation of the hybrid yarns clearly indicates their intrinsic humidity-sensing ability. In our experiment, the paddle fixed at the free end exhibited rotation instantaneously (see Video S7†) even when a bare finger approached but did not touch the yarn, with the torsional direction similar to that of the direct contact with water, which may be attributed to the adsorption of finger-evaporated sweat vapours. In contrast, the opposite rotation occurred if the finger was covered with dry gloves owing to some water loss of the yarn caused by body temperature,

which, along with the former observation, eliminated the possibility of electrostatic interactions. We quantitatively investigated the relationship between the paddle rotation and relative humidity by placing the freely suspended yarn-with-paddle configuration into a homemade humidity chamber (18%–41.9% RH, $24.0 \pm 0.3 \text{ }^\circ\text{C}$, Fig. 5a, S8 and S9†). As displayed in Fig. 5b, the rotation angle shows an approximately linear relationship with the gradual variation of surrounding humidity, and the sensitivity is estimated to be $74.3 \text{ degree}/1\% \text{ RH}$ for the specific combination of the yarn (29 mm long, 7736 turns per m) and paddle ($I = 2.8 \times 10^{-9} \text{ kg m}^2$), which hint at their possible applications as humidity sensors or switches. A small but noticeable deviation in the angle between the humidity increase and decrease process could mainly arise from temperature or gas flow perturbation, precision accuracy ($\pm 3\% \text{ RH}$) of the hygrometer and inevitably non-ideal distribution of humidity in the chamber. A more stable and controllable environmental humidity with a wider variation range is needed to thoroughly examine and gain more understanding about these observations, which will be our future work. As another demonstration (Fig. 5c and Video S8†), we wove the hybrid yarns into a smart fabric, which could lift a weight driven by humidity or water.

The temperature-triggered reverse rotation furthermore enlightened us to actuate the hybrid yarns through Joule heating, considering that both CNT and PEDOT:PSS are electrically conductive. As depicted in Fig. 5d and Video S9†, two hybrid yarns with opposite chirality (note that identical chirality should have a contradictive effect) were connected in series by a copper paddle ($I = 3.7 \times 10^{-10} \text{ kg m}^2$), which brought about a quick rotation when the electric current (10 mA for $\sim 1 \text{ s}$) was turned on and rotated back once the current was off.

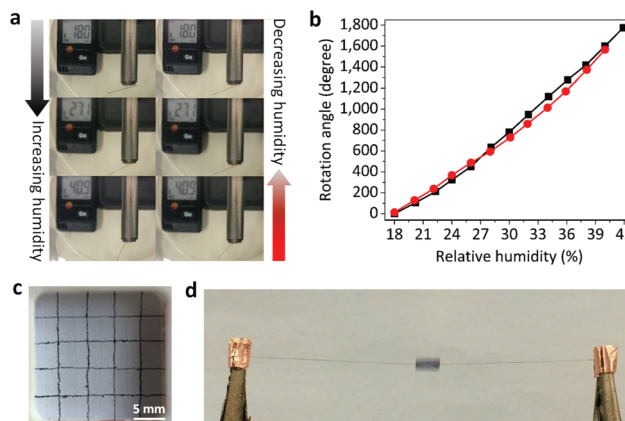


Fig. 5 (a) Paddle's position in the humidity chamber. The paddle rotates anticlockwise when the humidity increases, and rotates in a reverse direction when humidity decreases. (b) Dependence of the rotation angle on the relative humidity in the chamber. Black squares and red circles are for the humidity increase and decrease process, respectively. (c) A smart fabric made by weaving eight hybrid yarns. (d) Actuation under the excitation of electric current. A copper paddle is suspended by two yarns with opposite chirality and reveals a quick rotation when a short ($\sim 1 \text{ s}$) current pulse of 10 mA is applied.

The hybrid yarns driven by the pulsed current, alternating between the dry and the wet state and rendering the rotation in a forward and reverse rhythm, may be suitable for some special applications, *e.g.*, microfluidic mixers, although the torsional stroke is not large on account of low ambient humidity (~18% RH) which is less sufficient for efficient swelling and motility.

The guest material PEDOT:PSS endows the composite yarns with excellent hydro-actuation capability, due to its strong hygroscopicity that basically originates from PSS as a typical hydrophilic polyelectrolyte bearing sulfonic acid groups.^{28–30} In one previous study, a PEDOT:PSS film shows a volume increase of 4.5% with change in humidity from 20% to 90% RH,²⁹ and more osmotic expansion³¹ can be anticipated if the film directly touches liquid water. Besides the high moisture sensitivity and water harvesting capability of the selected PEDOT:PSS, impressive hydro-driven actuation significantly benefits from the helical structure of the motor-twisted yarns that can reversibly twist and untwist, as well as the large specific surface area supplied by nano-scale pores and channels which provide plenty of sites for water uptake and diffusion. In light of these characteristics, the hybrid yarns undergo water adsorption and volume expansion when they sense moisture, which transduces the free-energy change of the whole system directly into mechanical work.³² Conversely, dimensional shrinkage and backward rotation occur due to water desorption resulting from heat or negative humidity gradient. The simultaneously generated lengthwise contraction could be interpreted as Poisson's effect.

The actuation performance mainly depends on factors including the twist density of the yarns, the moment of inertia or the applied stress of the paddles. Particularly, coiled yarns with a larger twist density are extremely helpful to amplify the contraction output. The quantity and speed of water supply also play an important role. In rotation-involved experiments, the recovery generally took more time than the actuating process, probably ascribed to slower evaporation of water under ambient conditions and reduced stiffness²⁸ in the water swollen state (Fig. S7†), whereas porous channels and friction between nanotubes or/and PEDOT:PSS molecules are expected to assist in desorption. Besides, the hybrid yarns exhibit little response to ethanol differing from pure CNT yarns, which implies full coating of PEDOT:PSS on nanotubes, although our infiltration method could not guarantee the uniformity in the sense that the coating thickness should be smooth and homogeneous on each CNT or CNT bundle.

The stability of the cured PEDOT:PSS film in water has been rarely studied. But after being soaked in water for nearly three months, the film neither fell apart nor dissolved, perhaps because the entangled long chains of PEDOT are difficult to be separated. In contrast, the PDDA film has easily dissolved after being soaked in water for several minutes. Moreover, as displayed in Fig. S10,† after being soaked in water for 24 hours, the CNT/PDDA hybrid yarn degrades obviously, while the performance of the CNT/PEDOT:PSS hybrid yarn is almost not influenced.

Conclusions

In summary, hydro-driven CNT/PEDOT:PSS hybrid yarn muscles have been successfully constructed with a facile process, which display great capacity of rotation and contraction as well as a versatile way of actuation. The total torsional stroke is up to 4240 revolutions per m at a paddle-to-yarn mass ratio of 3300 and the contractive strain reaches 68% with an applied stress of 1 MPa. Approximately linear response to humidity changes and electromechanical actuation is also demonstrated. These as-prepared smart yarns are believed to be promising candidates for practical applications such as artificial muscles, hydro-driven generators, moisture switches and microfluidic mixers. Additionally, as with CNT/paraffin wax composite muscles,² the hybridization concept is illuminating for other functional CNT yarns that take full advantage of their extraordinary properties to offer diverse and useful locomotion.

Experimental

Preparation of the hybrid yarns

First, a freestanding film was clamped between two pieces of weighing paper and cut with a bistoury to obtain pieces of narrow ribbons (3–5 mm wide). The ribbons were then soaked in the ethanol solution where the weighing paper was readily peeled off. A commercially available PEDOT:PSS aqueous dispersion (Clevios PH 1000, 1:2.5 PEDOT:PSS ratio, solid content 1.0%–1.3%; H.C. Starck GmbH) was mixed with 1 wt% of the fluorosurfactant Zonyl-FS300 (Sigma-Aldrich). Subsequently, the CNT ribbon was immersed in a drop of the as-prepared PEDOT:PSS aqueous solution on a glass substrate and immediately drawn out. Before it was dried in the air, the infiltrated ribbon was suspended at a motor to controllably insert twists with a weight fixed at the free end. Theoretically, the weight and the motor-twisting speed could be tuned to obtain yarns with different helical angles, which is beyond the scope of this study. A block was employed to impede rotation of the weight during the motor-twisting process. Finally, the hybrid yarn was annealed at 120 °C for 30 min. The content of PEDOT:PSS in the hybrid yarn was determined to be around 60–70 wt% by measuring the mass of pristine and infiltrated ribbons under ambient conditions. When the pristine CNT ribbons were directly motor-twisted and then infiltrated by using the PEDOT:PSS aqueous solution, hybrid yarns with a core-shell structure (Fig. S3c and d†) were obtained. The CNT/PDDA hybrid yarns were prepared using the same process as the CNT/PEDOT:PSS hybrid yarns, except that these yarns were cured under ambient conditions. The PDDA aqueous dispersion (M_w 200 000–350 000, 20 wt%) was purchased from Aladdin Industrial Corp.

Characterization

SEM morphologies were examined using a Hitachi S5200 SEM system operated at 5 kV. The cross-section was obtained by cutting the hybrid yarn along its diameter with Ga ions (2.5 nA

beam current) in a FEI Helios 600i FIB/SEM system operated at 30 kV. A Keyence LK-H050 laser displacement sensor was utilized to track and record the rotation of the paddle. The current during the electrically-induced actuation was applied by using a Keithley 2400 Source Meter. The ambient temperature and humidity conditions were monitored and recorded by using a Testo 174H hygrometer. Mechanical tests of the pristine and hybrid yarns (Fig. S7†) were performed in a TA Instruments Dynamic Mechanical Analyzer Q800 on specimens with the same gauge length of 10 mm and force rate of 0.01 N min⁻¹. The specimens were prepared by straightly and tightly pasting them onto paper frameworks at both ends for convenient manipulation.

Acknowledgements

This work was supported by the National Basic Research Program of China (Grant No. 2012CB932302), the National Natural Science Foundation of China (51172271 and 51372269), and the “Strategic Priority Research Program” of the Chinese Academy of Sciences (XDA09040202).

Notes and references

- J. Foroughi, G. M. Spinks, G. G. Wallace, J. Oh, M. E. Kozlov, S. Fang, T. Mirfakhrai, J. D. W. Madden, M. K. Shin, S. J. Kim and R. H. Baughman, *Science*, 2011, **334**, 494–497.
- M. D. Lima, N. Li, M. J. de Andrade, S. Fang, J. Oh, G. M. Spinks, M. E. Kozlov, C. S. Haines, D. Suh, J. Foroughi, S. J. Kim, Y. Chen, T. Ware, M. K. Shin, L. D. Machado, A. F. Fonseca, J. D. W. Madden, W. E. Voit, D. S. Galvao and R. H. Baughman, *Science*, 2012, **338**, 928–932.
- M. Schulz, *Science*, 2012, **338**, 893–894.
- W. Guo, C. Liu, F. Zhao, X. Sun, Z. Yang, T. Chen, X. Chen, L. Qiu, X. Hu and H. Peng, *Adv. Mater.*, 2012, **24**, 5379–5384.
- K. Y. Chun, S. Hyeong Kim, M. Kyoong Shin, C. Hoon Kwon, J. Park, Y. Tae Kim, G. M. Spinks, M. D. Lima, C. S. Haines, R. H. Baughman and S. Jeong Kim, *Nat. Commun.*, 2014, **5**, 3322.
- J. A. Lee, Y. T. Kim, G. M. Spinks, D. Suh, X. Lepro, M. D. Lima, R. H. Baughman and S. J. Kim, *Nano Lett.*, 2014, **14**, 2664–2669.
- J. Yuan and P. Poulin, *Science*, 2014, **343**, 845–846.
- M. D. Lima, M. W. Hussain, G. M. Spinks, S. Naficy, D. Hagenasr, J. S. Bykova, D. Tolly and R. H. Baughman, *Small*, 2015, **11**, 3113–3118.
- C. H. Kwon, K. Y. Chun, S. H. Kim, J. H. Lee, J. H. Kim, M. D. Lima, R. H. Baughman and S. J. Kim, *Nanoscale*, 2015, **7**, 2489–2496.
- P. N. Chen, Y. F. Xu, S. S. He, X. M. Sun, S. W. Pan, J. Deng, D. Y. Chen and H. S. Peng, *Nat. Nanotechnol.*, 2015, **10**, 1077–1083.
- S. He, P. Chen, L. Qiu, B. Wang, X. Sun, Y. Xu and H. Peng, *Angew. Chem., Int. Ed.*, 2015, **54**, 14880–14884.
- S. H. Kim, C. H. Kwon, K. Park, T. J. Mun, X. Lepro, R. H. Baughman, G. M. Spinks and S. J. Kim, *Sci. Rep.*, 2016, **6**.
- S. H. Lee, T. H. Kim, M. D. Lima, R. H. Baughman and S. J. Kim, *Nanoscale*, 2016, **8**, 3248–3253.
- T. Mirfakhrai, J. Oh, M. Kozlov, E. C. W. Fok, M. Zhang, S. Fang, R. H. Baughman and J. D. W. Madden, *Smart Mater. Struct.*, 2007, **16**, S243–S249.
- D. Q. Yang, J. F. Rochette and E. Sacher, *J. Phys. Chem. B*, 2005, **109**, 4481–4484.
- W. Ma, L. Song, R. Yang, T. Zhang, Y. Zhao, L. Sun, Y. Ren, D. Liu, L. Liu, J. Shen, Z. Zhang, Y. Xiang, W. Zhou and S. Xie, *Nano Lett.*, 2007, **7**, 2307–2311.
- J. Li, W. Ma, L. Song, Z. Niu, L. Cai, Q. Zeng, X. Zhang, H. Dong, D. Zhao, W. Zhou and S. Xie, *Nano Lett.*, 2011, **11**, 4636–4641.
- Z. Niu, H. Dong, B. Zhu, J. Li, H. H. Hng, W. Zhou, X. Chen and S. Xie, *Adv. Mater.*, 2013, **25**, 1058–1064.
- N. Zhang, P. S. Luan, W. Y. Zhou, Q. Zhang, L. Cai, X. Zhang, W. B. Zhou, Q. X. Fan, F. Yang, D. Zhao, Y. C. Wang and S. S. Xie, *Nano Res.*, 2014, **7**, 1680–1690.
- N. Zhang, W. Y. Zhou, Q. Zhang, P. S. Luan, L. Cai, F. Yang, X. Zhang, Q. X. Fan, W. B. Zhou, Z. J. Xiao, X. G. Gu, H. L. Chen, K. W. Li, S. Q. Xiao, Y. C. Wang, H. P. Liu and S. S. Xie, *Nanoscale*, 2015, **7**, 12492–12497.
- L. Cai, J. Li, P. Luan, H. Dong, D. Zhao, Q. Zhang, X. Zhang, M. Tu, Q. Zeng, W. Zhou and S. Xie, *Adv. Funct. Mater.*, 2012, **22**, 5238–5244.
- L. Cai, L. Song, P. Luan, Q. Zhang, N. Zhang, Q. Gao, D. Zhao, X. Zhang, M. Tu, F. Yang, W. Zhou, Q. Fan, J. Luo, W. Zhou, P. M. Ajayan and S. Xie, *Sci. Rep.*, 2013, **3**.
- A. C. Keefe and G. P. Carman, *Smart Mater. Struct.*, 2000, **9**, 665–672.
- J. Kim and B. Kang, *Smart Mater. Struct.*, 2001, **10**, 750–757.
- Y. Fang, T. J. Pence and X. Tan, *Trans. Mechatronics*, 2011, **16**, 656–664.
- T. Mirfakhrai, J. D. W. Madden and R. H. Baughman, *Mater. Today*, 2007, **10**, 30–38.
- H. Cheng, Y. Hu, F. Zhao, Z. Dong, Y. Wang, N. Chen, Z. Zhang and L. Qu, *Adv. Mater.*, 2014, **26**, 2909–2913.
- H. Okuzaki, H. Suzuki and T. Ito, *J. Phys. Chem. B*, 2009, **113**, 11378–11383.
- H. Okuzaki, H. Suzuki and T. Ito, *Synth. Met.*, 2009, **159**, 2233–2236.
- S. Taccola, F. Greco, E. Sinibaldi, A. Mondini, B. Mazzolai and V. Mattoli, *Adv. Mater.*, 2015, **27**, 1668–1675.
- L. Bay, T. Jacobsen, S. Skaarup and K. West, *J. Phys. Chem. B*, 2001, **105**, 8492–8497.
- H. Okuzaki, T. Kuwabara, K. Funasaka and T. Saido, *Adv. Funct. Mater.*, 2013, **23**, 4400–4407.